Alkaline-Earth Oxide Nanoparticles Obtained by Aerogel Methods. Characterization and Rational for Unexpectedly High Surface Chemical Reactivities

Olga B. Koper, Isabelle Lagadic, Alexander Volodin, and Kenneth J. Klabunde*

Department of Chemistry, Kansas State University, Manhattan, Kansas 66506

Received May 12, 1997. Revised Manuscript Received September 23, 1997[⊗]

Aerogel preparation of MgO and CaO nanoparticles involves a sol−gel approach where methoxides are converted to hydroxide gels followed by hypercritical drying and vacuum dehydration. This produces, for these particular hydroxides/oxides, ultrafine particulates rather than monoliths. These particulate materials have exhibited unexpectedly high surface chemical reactivities that have allowed their successful use as high-capacity destructive adsorbents for toxic chemicals, including chlorocarbons, organophosphorus compounds, and acid gases. Detailed characterization involving X-ray diffraction (XRD), gas adsorption/pore distribution analysis, infrared, TEM, AFM, XPS, probe molecule adsorption, and elemental analysis has allowed a rationale to be developed that helps explain the high chemical reactivities observed, especially for CaO. Pore volume and size distribution, unusual surface morphologies with a high ratio of edge ion/surface ions, and trace residual (persistent) surface −OH and $-OCH_3$ seem to be the main factors allowing these nanoparticulates to be isolable and stable and yet highly reactive, and results for CaO are emphasized herein.

I. Introduction

A. Aerogel Background. The aerogel−hypercritical drying synthetic approach to metal oxides was first developed by Kistner in 1932 for preparation of high surface area silica.[1] While working on inorganic gels he showed that during the dehydration process under normal conditions a disruption of the pore structure occurs, destroying the gel network. However, if a supercritical pressure and temperature were used during the drying procedure, the structure did not collapse. After preliminary experiments Kistner wrote "the liquid in jelly can be replaced by gas with little or no shrinkage".[2] Silica gels were prepared by hydrolyzing water glass with hydrochloric acid. The gel was dried in an autoclave where the liquid in the gel was held under a pressure larger than its vapor pressure. With increasing temperature the liquid at its critical temperature was transformed into a fluid. The gel was dried by replacing the interstitial fluid with a dry gas. Under these conditions liquid−vapor phases do not exist; hence, there is no surface tension or capillary pressure that would lead to a collapse in the gel structure. The residual solvent could be removed by flushing an inert gas through the hot solid, thus yielding an aerogel. The major drawback of this procedure was the long and tedious preparation. In 1962 the French government asked Teichner to design a method for storing oxygen and rocket propellants in porous materials.[3] He tried to use Kistner's method, but because more than a week was required to prepare one sample, he decided to modify the procedure. To speed up the process Teichner and co-workers[4,5] started to use organic solvents instead of water. First they dissolved tetramethoxysilane (TMOS) in methanol and hydrolyzed it with a controlled amount of water.[4,6]

$$Si(OCH_3)_4 + 4H_2O \xrightarrow{MeOH} SiO_2{\cdot}2H_2O + 4CH_3OH$$

This substitution decreased the preparation time to a few hours and yielded alcogel free of impurities, that was subsequently dried in an autoclave giving extremely high surface area (1000 m^2/g) silica aerogel.[6]

The factors that influence the appearance and properties of the final aerogel are: the degree of hydrolysis, the nature of the metal and polarity of M−O−C bond, the number and the nature of alkoxyl groups, solvent, dilution, time of gelation, pH, and temperature.[2,3] The metal oxide products−aerogels are very porous materials with low densities, a large number of defect sites, extremely low conductivities and sound velocity (below 100 m/s) and very high surface area. Depending on the material, surface areas can range as high as 1200 m^2/g. Aerogels can be either translucent or transparent depending on the synthesis conditions.

Applications of aerogels are very large and diverse. They are used in Cerenkov radiators as detectors to identify the charge of high-energy particles and to measure their velocity. Transparent silica aerogels cover the range of refractive indices between 1.01 (gases) and 1.2 (liquids), and this is difficult to achieve using other materials.[4] This finding in 1974 has led to renewed interest in aerogels and to extensive studies in the past 2 decades.[2] Other applications are as gellifying rocket propellants, insulators in dual-pane

[⊗] Abstract published in *Advance ACS Abstracts,* November 1, 1997.

(1) Kistner, S. S. *J. Phys. Chem.* **1932**, *36*, 52.
(2) Gesser, H. D.; Goswami, P. C. *Chem. Rev. (Washington, D.C.)* **1989**, *89*, 765 and references therein.
(3) Zarzycki, J.; Woignier, T. *Aerogels*; Fricke, J., Ed.; Springer-Verlag: Berlin, 1985; p 42.
(4) Teichner, S. J. *Aerogels*; Fricke, Ed.; Springer-Verlag: Berlin, 1985; p 22.5.
(5) Nicolaon, G. A.; Teichner, S. J. *Bull. Soc. Chim. Fr.* **1968**, 3107.
(6) Teichner, S. J.; Nicolaon, G. A.; Vicarini, M. A.; Gardes, G. E. E. *Adv. Colloid Interface Sci.* **1976**, *5*, 245.

S0897-4756(97)00357-8 CCC: $14.00

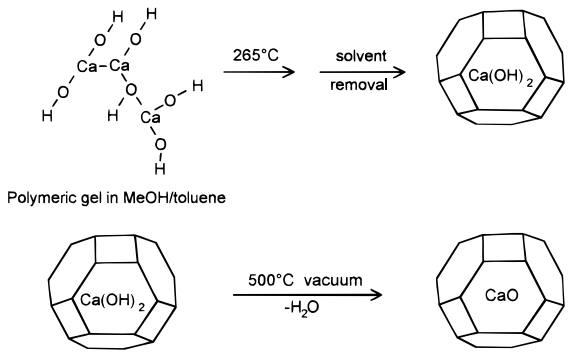

Figure 1. Collapse of polymeric $Ca(OH)_2$ gel during the hypercritical drying step.

windows, and insecticides. Recently, the most widely studied application of aerogels is in catalysis. For example, in Fischer−Tropsch catalysis, catalytic hydrogenation of carbon monoxide, Fe_2O_3/SiO_2, and Fe_2O_3/Al_2O_3 exhibit higher activity, by 2 or 3 orders of magnitude than the conventional reduced iron catalysts.[4]

As a further modification of the Kistner−Teichner aerogel method, large amounts of aromatic hydrocarbons have been added to alcohol−methoxide solution before hydrolysis and alcogel formation. This was done in order to further reduce the surface tension of the solvent mix and to facilitate solvent removal during the alcogel → aerogel transformation. [7−9] This led to two interesting developments:[7−11] (1) higher surface areas and smaller crystallite sizes for MgO, CaO, TiO_2, and ZrO_2 (herein referred to as AP samples for aerogel prepared) and (2) the formation of nanoparticulate free-flowing powders rather than monolithic aerogels. These findings indicate that during hypercritical drying of the gel, collapse does occur but with the formation of extremely small, stable nanocrystals, for example as shown in Figure 1 for calcium hydroxide, where the polymeric hydroxide segregates and forms tiny crystallites.

Since it is generally known that acid catalysis during gel formation leads to more linear chain polymer gels, while base catalysis leads to colloidal-like gels, it may not be surprising that the alkaline-earth hydroxides, being bases themselves, lead to particulates rather than monoliths. However, the very small crystallite sizes are rather remarkable, for example AP−MgO (~4 nm),[9] AP−CaO (7 nm),[9,12] AP−TiO_2 (10 nm),[10] AP−ZrO (8 nm).[11]

What is most intriguing is that these nanocrystals exhibit higher surface chemical reactivities than more conventionally prepared samples (simple precipitation of hydroxides followed by vacuum dehydration), herein labeled CP samples. For example, in the reaction $2CaO + CCl_4 \rightarrow 2CaCl_2 + CO_2$ aerogel prepared samples exhibited reaction efficiencies twice as high as CP−CaO and 30 times higher than commercial samples (CM−CaO).[9,12] In the adsorption of SO_2, AP−MgO adsorbed three times as much as CP−MgO/nm^2.[13] In the destructive adsorption of $CH_3(CH_3O)_2PO$ reaction efficiencies were 4 times greater for AP−MgO vs CP−MgO and 50 times greater than for CM−MgO.[14] Thus, this high reactivity has been exhibited in numerous reactions at both room temperature and elevated temperatures and *is not simply due to enhanced surface areas* (although this is also beneficial). There are intrinsic differences in surface reactivity, and herein extensive characterization studies are reported that allow some explanation for these findings. The data presented deal mainly with CaO, but some discussion of MgO is included. Extensive comparisons between AP−CaO (aerogel prepared) CP−CaO (conventionally prepared) and CM−CaO (commercially available) have been necessary in order to delineate the differences.

B. Calcium Oxide Background. Normally prepared by thermal decomposition of calcium carbonate,[15,16] CaO has been found to be useful as a catalyst for hydrogenation and isomerization of alkenes,[17,18] oxidative coupling of methane,[19] dehydrogenation of alcohols, H_2-O_2 and CH_4-O_2 exchange,[20] and other processes.[21] Also the ability of CaO to adsorb SO_2[22,23] and CO_2[24−27] is well-known.

Numerous reports dealing with the surface properties (basicity, acidity) of CaO have appeared.[28−41] One such

(7) Utamapanya, S.; Klabunde, K. J.; Schlup, J. R. *Chem. Mater.* **1991**, *3*, 175−181.
(8) Itoh, H.; Utamapanya, S.; Stark, J.; Klabunde, K. J.; Schlup, J. R. *Chem. Mater.* **1993**, *5*, 71.
(9) Klabunde, K. J.; Stark, J. V.; Koper, O.; Mohs, C.; Park, D. G.; Decker, S.; Jiang, Y.; Lagadic, I.; Zhang, D. *J. Phys. Chem.* **1996**, *100*, 12142−12153.
(10) Klabunde, K. J.; Stark, J. V.; Koper, O.; Mohs, C.; Khaleel, A.; Glavee, G.; Zhang, D.; Sorensen, C. M.; Hadjipanayis, G. C. *Nanophase Materials*; Hadjiapanayis, G. C., Siegel, R. W., Eds.; Kluwer Academic Publishers: The Netherlands, 1994; p 1.
(11) Bedilo, A.; Klabunde, K. J. *Nanostruct. Mater.* **1997**, *8*, 119−135.
(12) Koper, O.; Klabunde, K. J. *Chem. Mater.* **1993,** *5*, 500−505.
(13) (a) Stark, J. V.; Park, D. G.; Lagadic, I.; Klabunde, K. J. *Chem. Mater.* **1996**, *8*, 1904−1912. (b) Stark, J. V.; Klabunde, K. J. *Chem. Mater.* **1996**, *8*, 1913−1918.
(14) (a) Li, Y. X.; Koper, O.; Atteya, M.; Klabunde, K. J. *Chem. Mater.*, **1992,** *4*, 323−330. (b) Li, Y. X.; Klabunde, K. J. *Langmuir* **1991**, *7*, 1388−1393.
(15) Bellobono, I. R.; Castellano, L.; Tozzi, A. *Mater. Chem. Phys.* **1991**, *28*, 69.
(16) Bellobono, I. R.; Selli, E.; Righetto, L. *Mater. Chem. Phys.* **1988**, *19*, 131.
(17) Schächter, Y.; Pines, H. *J. Catal.* **1968,** *11*, 147.
(18) Albeck, M.; Rav-Acha, Ch.; Gil-Av, E.; Schächter, O. *J. Catal.* **1971**, *22*, 219. Hattori, H.; Satoh, A. *J. Catal.* **1976**, *45*, 32.
(19) Carreiro, J. A. S. P.; Baerns, M. *J. Catal.* **1989**, *117*, 258.
(20) Matsuda, T.; Sugimoto, M.; Yoshiara, H. *Bull. Chem. Soc. Jpn.* **1991**, *64*, 552.
(21) Tanabe, K. *Solid Acids and Bases*; Academic Press: New York, 1970.
(22) Allal, K. M.; Abbessi, M.; Mansour, A. *Bull. Soc. Chim. Fr.* **1991**, *128*, 880.
(23) Withum, J. A.; Yoon, H. *Environ. Sci. Technol.* **1989**, *23*, 821.
(24) Fukuda, Y.; Tanabe, K. *Bull. Chem. Soc. Jpn.* **1973**, *46*, 1616.
(25) Beruto, D.; Botter, R.; Searcy, A. W. *J. Phys. Chem.* **1984**, *88*, 4052.
(26) Philipp, R.; Fujimoto, K. *J. Phys. Chem.* **1992**, *96*, 9035.
(27) Philipp, R. P.; Omata, K.; Aoki, A.; Fujimoto, K. *J. Catal.* **1992,** *34*, 422.
(28) Iizuka, T.; Tanabe, K. *Bull. Chem. Soc. Jpn.* **1975**, *48(9)*, 2527.
(29) Paukshtis, E. A.; Soltanov, R. I.; Yurchenko, E. N. *React. Kinet. Catal. Lett.* **1982**, *19*, 105.
(30) Maciel, G. E.; Haw, J. F.; Chuang, I. S.; Hawkins, B. L.; Early, T. A.; McKay, D. R.; Petrakis, B. L. *J. Am. Chem. Soc.* **1983**, *105*, 5529.
(31) Dewing, J.; Monks, G. T.; Youll, B. *J. Catal.* **1976**, *44*, 226.
(32) Emeis, C. A. *J. Catal.* **1993**, *141*, 347.
(33) Itoh, H.; Utamapanya, S.; Stark, J.; Klabunde, K. J.; Schlup, J. R. *Chem. Mater.* **1993,** *5*, 71.
(34) Cusumano, J. A.; Low, M. J. D. *J. Phys. Chem.* **1970**, *74*, 792.
(35) Cusumano, J. A.; Low, M. J. D. *J. Catal.* **1971**, *23*, 214.
(36) Cusumano, J. A.; Low, M. J. D. *J. Colloid Interface Sci.* **1972**, *38*, 245.
(37) Echterhoff, R.; Knözinger, E. *Surf. Sci.* **1990**, *230*, 237.
(38) Sato, M.; Kanbayashi, T.; Kobayashi, N.; Shima, Y. *J. Catal.* **1967**, *7*, 342.
(39) Echterhoff, R.; Hoffman, P.; Knözinger, E. *Proceedings of the 9th International Congress on Catalysis*; Calgary, 1988; p 1418.
(40) Knözinger, E.; Jakob, K. H.; Singh, S.; Hoffman, P. *Surf. Sci.* **1993**, *290*, 288.

study using phenol vapor adsorption showed that CaO possesses strongly basic surface sites, whereas this probe indicated MgO and BeO to be moderate bases in comparison.

Three types of basic centers have been proposed to exist on the CaO surface: strongly basic O^{2-} centers (isolated) and adjacent to residual −OH groups, and weakly basic −OH groups.[21,42]

II. Experimental Section

A. Preparation of AP−CaO. This procedure has been described briefly before along with a reaction schematic.[9] A more detailed description is given here.

(1) Preparation of 10% Calcium Methoxide in Methanol Solution. $Ca(OCH_3)_2$ was obtained from calcium and methanol. First calcium metal pieces, stored under argon to prevent oxidation, were cleaned with acetone immediately before the reaction. Then, to a 500-mL round-bottom flask 8 g (0.2 mol) of calcium and 230 mL (182 g, 5.68 mol) of spectroanalyzed grade methanol were introduced. The reactants were stirred at room temperature for 16 h. To prevent exposure of the calcium methoxide to atmospheric moisture, the reaction was carried out under a slow flow of nitrogen gas. When the reaction started, formation of hydrogen bubbles on the calcium surface was observed. After all metal reacted the mixture was white and opaque. *(2) Hydrolysis of Calcium Methoxide.* A solution of calcium methoxide in methanol−toluene was hydrolyzed at room temperature overnight, by stirring 20 g (0.2 mol) of 10 wt % $Ca(OCH_3)_2$, 180 mL (156 g, 1.7 mol) of toluene, and 1.2 mL (0.07 mol) of triply distilled, deionized water in a 400-mL beaker. As the water was added, drop by drop, using a syringe, a white solid formed in the solution that slowly transformed to a clear gel. To prevent the mixture from evaporation, the beaker was covered with aluminum foil. After an hour an additional drop of water was added to make sure that all the methoxide had reacted. If a white solid was still formed, more water was added. Stirring was continued overnight. *(3) The Autoclave Treatment Procedure.* The hydroxide gel solution was transferred into the glass liner of a 600 mL Parr autoclave. The mixture was first flushed with nitrogen, and the reaction was carried out under nitrogen, with an initial pressure of 100 psi. The reactor was slowly heated from room temperature to 265 °C at 1 °C/min. Time of heating was about 4 h. After reaching the desired temperature, the reactor was held at 265 °C for 10 min. During heating the pressure inside the autoclave increased from 100 to 600 psi. The system was vented to the atmosphere, over a 5 min period, the furnace taken off, and the calcium hydroxide flushed with nitrogen for 10 min to remove the remaining organic solvents. The autoclave was then allowed to cool to room temperature over approximately 2 h. *(4) Thermal Conversion of Calcium Hydroxide into Calcium Oxide.* The $Ca(OH)_2$ sample was placed in a Schlenk tube and evacuated at room temperature for 30 min. Later, it was slowly heated (6 h) from room temperature to 500 °C and then kept under these conditions for 15 h at 1×10^{-3} Torr. Most of the water came off at 350 °C; therefore, the sample was kept at this temperature 2−3 h before continuing up to 500 °C. The slow heating prevented rapid outgassing of the sample and sintering. After the heat treatment, the Schlenk tube was closed and the sample was stored under inert atmosphere (in the glovebox) for future use. Calcium oxide obtained by this method had a surface area ranging from 120 to 160 m^2/g.

(B) Preparation of CP−CaO. To a 400-mL beaker, 10 g of CM−CaO and 150 mL of water were added, and the beaker was covered with a watch glass to avoid quick evaporation of the water. The slurry was heated to 80 °C and then kept at this temperature for 2 h (when the water was almost completely evaporated). Before each experiment CP−$Ca(OH)_2$ was activated under dynamic vacuum (1×10^{-3} Torr) at the desired temperature in a manner similar to that described for AP−CaO. Conventionally prepared calcium oxide had a surface area of 80−100 m^2/g.

(C) CM−CaO. A commercial calcium oxide sample (Fisher Scientific) was used without further treatment. The surface area of such an oxide was about 10 m^2/g.

(D) Methods for Characterization of the Oxides. *(1) Powder X-ray Diffraction (XRD).* For XRD studies about 0.5 g of calcium oxide was placed in a Schlenk tube and heated under vacuum to a desired temperature, 100, 200, 300, 350, 400, and 500 °C. At this temperature the powder was kept overnight and then, after cooling, transferred to the glovebox and under an inert atmosphere of argon, ground, covered with Nujol, and loaded onto the sample holder. X-ray diffraction patterns were recorded using a Scintag-XDS-2000 instrument. The spectrometer was set at a voltage of 40 kV and a current 40 mA. The scans were from 20° to 85° with a scanning rate of 2°/min. Using the XRD spectra, the crystallite size was calculated by measuring the peak widths at half-height and applying the Scherrer equation. *(2) Infrared Spectroscopy (FT-IR).* FT-IR was used to observe changes during dehydroxylation, as well as to identify gases coming off during this process. For analysis of the solid, calcium hydroxide was pressed into a tungsten grid and slowly heated from room temperature to the desired temperature under dynamic vacuum,[43,44] held for 15 min, and then cooled to room temperature, and an IR spectrum was taken. The sample was heated, and the spectra were taken without moving it out of the beam; therefore, the intensities shown corresponded to the same place on the sample. These experiments were conducted on an RS-1 FT-IR spectrometer from Mattson, with a liquid nitrogen cooled MCT detector.

For studying gases coming off during the heat treatment, about 3 g of the hydroxide was placed in a Schlenk tube, closed, and heated to a desired temperature at which time the evolved gases were transferred, using liquid nitrogen, to a gas IR cell and the spectrum taken. The instrument used was a FT-IR FTS-40 with a DTGS detector from Bio-Rad. *(3) Brunauer−Emmet−Teller Method (BET).* This method was used for measuring the surface areas of calcium oxide and hydroxide, using a Micromeritics FlowSorb II 2300 with a dual-channel system (900 Series, Sierra Instruments). The sample was first outgassed at 120 °C, to remove water adsorbed on the surface, and then exposed to N_2 gas. The quantity of nitrogen that adsorbed on a sample as a single layer was measured. From the number of adsorbed molecules and the area occupied by each, the surface area was directly calculated. The preferred gas mixture for a monolayer formation was 30% volume of N_2 and 70% of He. The adsorption was done at the boiling point of nitrogen.

Similar studies were carried out using a vacuum line (Figure 2) to measure the surface area without exposing the heat-treated sample to the air and later to measure the number of hydroxyl groups on the surface, which were quantitatively determined by reaction with triethylaluminum.[8] *(4) Thermogravimetric Analysis (TGA).* These studies were conducted under a flow of air or helium as well as under vacuum. To measure the weight loss under gas flow, the calcium hydroxide powder was placed in a minibasket and heated from room temperature to 900 °C with a heating rate of 20 °C/min using a thermogravimetric analyzer TGA-50 from the Shimadzu Co. The weight loss was recorded with respect to the temperature increase. To measure the weight loss under vacuum, a quartz spring balance with an accuracy of ±0.5 mg was used.[12] *(5) Elemental Analysis.* Calcium oxide was heat treated under vacuum at 500 °C overnight, transferred into glass vials in an argon atmosphere, and sent to the Galibraith Laboratories (Knoxville, TN) for analysis. Elemental analysis was conducted for calcium, hydrogen, and carbon. The amount of

(41) Knözinger, H.; Ratnasamy, P. *Catal. Rev. Sci. Eng.* **1978**, *17*, 31.

(42) Iizuka, T.; Hattori, H.; Yasuhiro, O.; Sohma, J.; Tanabe, K. *J. Catal.*, **1971**, *22*, 130.

(43) Koper, O.; Wovchko, E. A.; Glass, J. A.; Yates, J. T., Jr.; Klabunde, K. J. *Langmuir* **1995**, *11*, 2054−2059.

(44) Basu, P.; Ballinger, T. H. Yates, J. T., Jr. *Rev. Sci. Instrum.* **1988**, *59*, 1321.

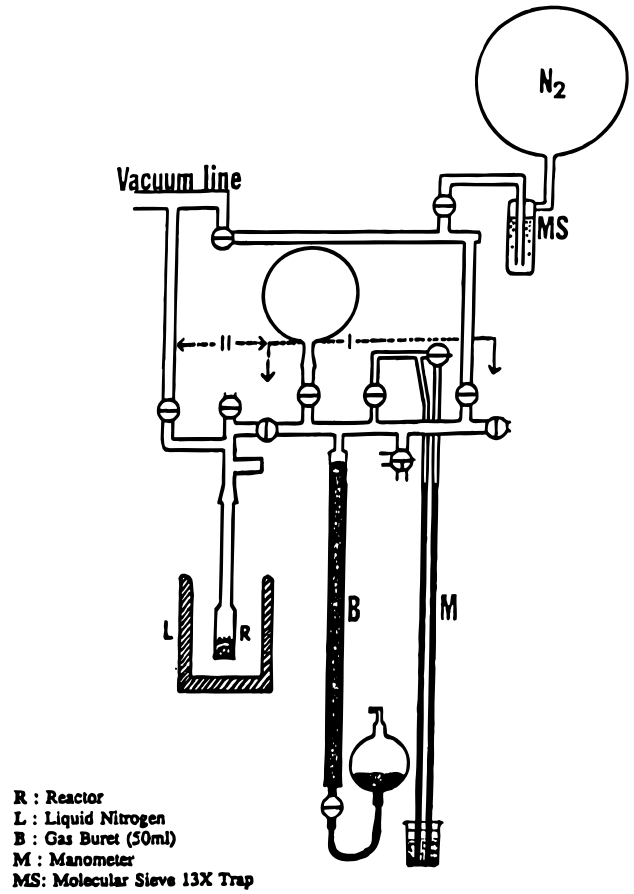

Figure 2. Schematic diagram of vacuum system used for surface hydroxyl group titration, and some surface area measurements.

oxygen was obtained by summing the amounts of Ca, C, and H and subtracting it from 100. *(6) Electron Probe Microanalysis (EPMA).* In the EPMA experiment a selected area of the sample is bombarded with a beam of electrons, which causes the emission of an X-ray spectrum that consists of characteristic X-ray lines of elements present on the surface.[45] During the analysis the X-ray spectrum is dispersed and the wavelengths as well as intensities for each characteristic line are measured. Prior to the measurement, CaO preheat treated at 500 °C was pressed onto an indium metal sample, using a hydraulic press with a pressure of 3000 psi. First the SEM picture of the analyzed area was taken, and then photomicrographs for calcium, oxygen, and carbon were obtained, which represent the number of counts for each element. *(7) X-ray Photoelectron Spectroscopy (XPS or ESCA Electron Spectroscopy for Chemical Analysis).* XPS was used to observe differences in the surface composition for CP− and AP−CaO.[45,46] The elements studied were calcium, carbon, and oxygen. Prior to the measurement the powder was pressed onto indium metal to obtain a uniform layer of the oxide. The X-ray photoelectron spectra were taken with shorter and longer exposure to the X-rays (in case of CP−CaO) to determine the damage to the sample upon irradiation. The instrument used was AEI (Kratos) ES200 with a base pressure 10^{-8}−10^{-10} Torr. The spectrometer was operated in the FRR mode with Mg $K\alpha_{1,2}$ X-ray radiation source. The XPS data were collected on an IBM PC computer and then analyzed. The collection time for C 1s, O 1s, and Ca 2p was 10−30 min and for the valence band 12 h. The instrument was calibrated with the residual hydrocarbon on the surface, with the binding energy of 284.6 eV. The curve fitting was carried out using a nonlinear least-squares curve-fitting program with a Gaussian/Lorentzian mix of 0.5.[47] *(8) Total Pore Volume and Pore Size Distribution.* Total pore volume is calculated based on the "Gurvitsch rule", which states that the volume of the liquid condensed in the pores of a porous solid from a condensable gas near its saturation vapor pressure equals the volume of the pores.[27] Pore area and volume distribution were obtained from the desorption branch of an isotherm relating the amount of adsorbate lost in a desorption step to the average pore size of the pore emptied in that step.[27] These studies for conventional and aerogel-prepared oxides were conducted in a Micromeritics Instrument on a Gemini 2360 analyzer. Prior to the measurements both samples were heat treated under vacuum at 500 °C and sealed under argon. *(9) Transmission Electron Microscopy and Scanning Electron Microscopy.* Calcium oxide CP− and AP− samples were heat treated under vacuum at 500 °C overnight and transferred to an inert atmosphere box. To the powder freshly distilled solvents were added. The solvents used were absolute ethanol, acetone, toluene, and pentane. The TEM pictures were taken with and without sonication; the sonication time for ethanol, acetone, and toluene was 3 min. The best solvent proved to be pentane, and after addition of the solvent the resulting slurry was sonicated for 10, 30, and 60 min to achieve a better separation of the particles, prior to the measurement. The Microscope used was a Philips EM201. The magnification used was 44 600. SEM was conducted only on AP−CaO. The sample was dispersed in ethanol and placed onto a bare silicon substrate to eliminate surface artifacts from the support material. The specimens were uncoated and studied utilizing 1 kV accelerating voltages. The images were obtained by Bill Roth from Nissei Sangyo America, Ltd. on a high-resolution FESEM Model S-4500. *(10) Atomic Force Microscopy.* Imaging the sample surface was carried out using a commercial AFM (SPM 30 from Wyco Inc.) in the contact mode. A 100 nm long and rectangular cantilever with a spring force constant of 0.37 N/m and a Si_3N_4 integrated pyramidal tip was used. The force intensity was about $(8-15) \times 10^{-8}$ N, and the sample surfaces were scanned using the height mode, where the force and hence the distance between the tip and the surface is kept constant. All pictures were obtained in air at room temperature. Resolution was 256 × 256 pixels. This experimental condition was sometimes a drawback as the compounds are hygroscopic. The AFM experiments were carried out on different parts of the surface to make sure that the observed structure was representative and reproducible. Whenever it was possible, the powdered samples were put on an adhesive tape and slightly packed down with a spatula. Otherwise, the samples were studied after pressing the powder into a pellet under a pressure as low as possible (20×10^6 Pa). The preparation prior to imaging is indicated in the figure captions. The CM−CaO samples were observed without heat treatment. All other samples (CP− and AP−CaO) were heat treated overnight under vacuum at 500 °C and then cooled to room temperature before AFM observation. *(11) Acidity and Basicity.* To determine the acidity of the oxide, adsorption of a gaseous base, freshly distilled, freeze−thawed degassed pyridine, was employed. A quartz spring microbalance was used.[12] A minibasket containing calcium hydroxide (about 0.15 g) was attached to the quartz spring balance. The sample was heated to 500 °C and kept at this temperature under dynamic vacuum overnight. The temperature was regulated using a temperature controller with a thermocouple. The sample was then cooled, and pyridine vapors (under the pressure of 4 Torr) were introduced under a static vacuum. After 15 min of adsorption the sample was evacuated for 100 min. The differences in the weight of the sample, during the adsorption, caused changes in the length of the spring that allowed determination, by comparing it to a calibration curve, of the amount of adsorbed material. This system allowed measurement of changes in weight ±0.1 mg. To determine the basicity of the oxide a gaseous Lewis acid, carbon dioxide, was adsorbed

(45) *Practical Surface Analysis, 2nd ed.;* Briggs, D., Seah, M. P., Eds.; Wiley: Chichester, 1990; Vol. 1.

(46) *Handbook of X-Ray Photoelectron Spectroscopy*; Mullenberg, G. E., Ed.; Perkin-Elmer Corp.: Eden Prarie, MN, 1979.

(47) Thomas, S.; Sherwood, P. M. A. *Surf. Interface Anal.* **1993**, *20*, 595.

in the same manner as described for pyridine. The only difference was the pressure used, 10 Torr instead of 4 Torr.

III. Results

A. Preparation of AP−CaO(OH)$_2$ of Highest Surface Area. Many experiments were carried out in an attempt to maximize the surface area of the AP−Ca(OH)$_2$ obtained. As discussed earlier, a modified sol−gel approach was used where an alcogel was prepared in a methanol−toluene solvent mix followed by hypercritical drying to yield an aerogel (actually nanoscale particulates).

$$Ca + CH_3OH \xrightarrow{CH_3OH} (CH_3O)_2Ca + H_2 \qquad (1)$$

$$(CH_3O)_2Ca/CH_3OH \xrightarrow[(2)\ H_2O]{(1)\ \text{toluene}} Ca(OH)_2\ \text{(alcogel)}$$

$$Ca(OH)_2\ \text{(alcogel)} \xrightarrow[\text{drying (solvent removed)}]{\text{hypercritical}} Ca(OH)_2\ \text{(aerogel)}$$

Variations in the amounts of toluene and water, stirring time, and type of alcohol solvent (methanol or 1-butanol) were studied. Surface areas ranged from about 30 to 160 m^2/g. Highest surface areas were obtained with the following mole ratios: $(CH_3O)_2Ca:CH_3OH:C_6H_5CH_3:H_2O$ = 1:28:85:3.5.

It should be noted that a large amount of the relatively nonpolar solvent toluene has a beneficial effect. If the mole ratio of $Ca(OCH_3)_2$ to toluene was decreased to 1:40, the surface area of the Ca(OH)$_2$ dropped to about 60 m^2/g. If the stirring time (hydrolysis step) was decreased from 15 to 0.5 h, the surface area dropped to 30 m^2/g.

B. Heat Treatment Ca(OH)$_2$ → CaO Dehydration. *1. Solids.* Two methods were used to dehydrate the Ca(OH)$_2$. Heating in an oven at atmospheric pressure caused the surface areas to decrease from 100 m^2/g → 40 (300 °C), 40 (400 °C), or 35 m^2/g (500 °C). However, by dehydrating under dynamic vacuum surface areas actually increased to 140 (300 °C), 150 (400 °C), or 140 m^2/g (500 °C). Obviously it is important to rapidly remove the water vapor as it is formed to avoid sintering.

Infrared studies of the dehydration process are summarized in Figure 3, and the presence of residual surface −OH, −OCH$_3$, and carbonates is evident. Two types of −OH are present as shown near 3500 cm^{-1}. Assignment of these bands is controversial, but here we will use the nomenclature and models proposed by Knözinger.[37,39] That is, if the −OH group is attached to a Ca^{2+} ion of low coordination, the ν(O−H) will occur at higher frequency. On the basis of this model and the data of Knözinger for MgO,[37] we assign the higher energy ν(O−H) at 3676 cm^{-1} to a multiply coordinated isolated hydroxyl (1) and 3644 cm^{-1} to hydrogen-bonded −OH (2).

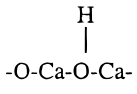

1

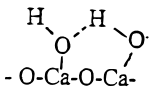

2

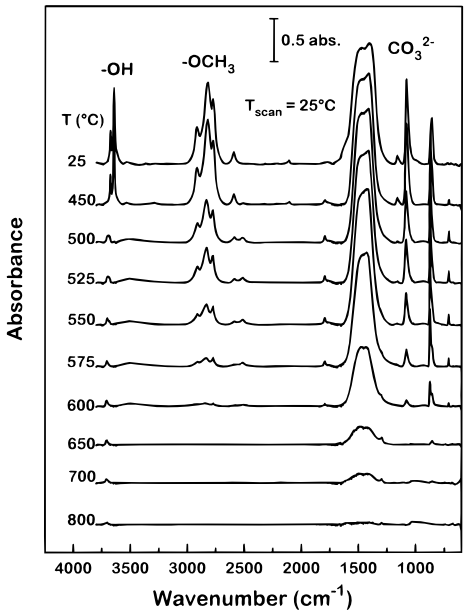

Figure 3. IR Bands observed during dehydration AP−Ca(OH)$_2$ → AP−CaO, 25−800 °C.

The small band near 3500 cm^{-1} is very likely due to physisorbed water. After heating the sample under vacuum to 500 °C, the hydrogen-bonded −OH groups disappeared and a new band due to isolated −OH (3710 cm^{-1}) appeared, and this band persisted up to 800 °C. Another prominent series of bands was observed between 2750 and 2900 cm^{-1} which is mainly due to residual −OCH$_3$ but could also be partly due to linearly bound CO$_2$.[39]

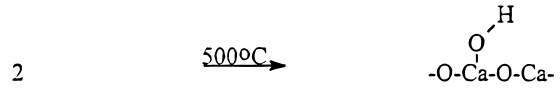

3

Due to brief exposure to air during sample handling at various stages, some CO$_2$ was adsorbed by these reactive materials. Therefore, a series of bands due to surface carbonate was also observed. After consideration of literature,[13,20,24,26,27] we assign the prominent band near 1500 cm^{-1} to symmetric stretching of unidentate carbonate:

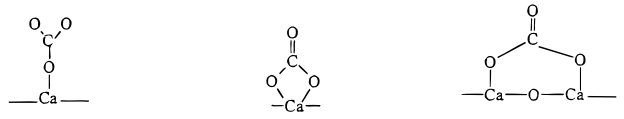

and the 1069 cm^{-1} band to CO_{II} stretching of unidentate carbonate. The 860 cm^{-1} band is probably due to a bridging type carbonate, and interestingly this band was much more prominent on CP−CaO (Figure 4).

The dehydration process was also followed by XRD, and both AP−Ca(OH)$_2$ and CP−Ca(OH)$_2$ were dehydrated between 300 and 350 °C. At 400 °C only CaO crystallites were present. Crystallite sizes were monitored and are plotted in Figure 5. Note that the AP−Ca(OH)$_2$ began at 13 nm, and as CaO was formed crystallites of CaO stabilized at about 7 nm. In the case

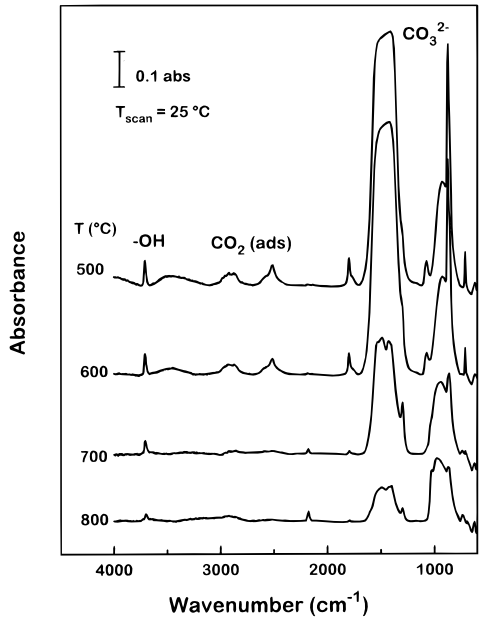

Figure 4. IR bands observed during dehydration CP−Ca-$(OH)_2$ → CP−CaO, 500−800 °C. (Spectra at 25−400 °C were similar to the 500 °C scan except a larger broad band at 3500 cm^{-1} due to associated OH was present.)

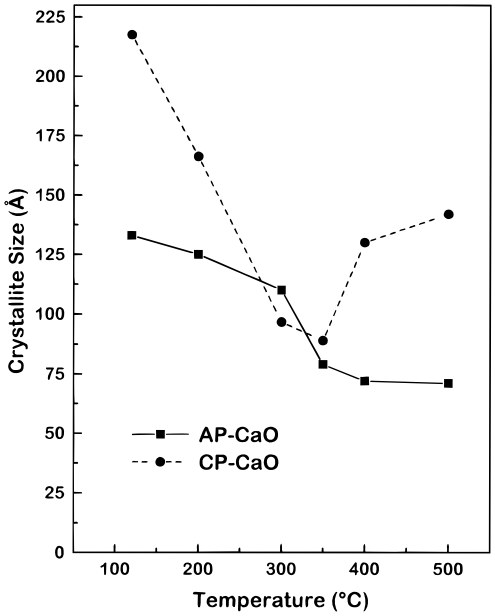

Figure 5. Crystallite size changes during heat treatment of CP− and AP− samples.

of CP−$Ca(OH)_2$, size decrease proceeded on heating to 350 °C, but then sintering began to occur, and crystallite size increased, indicating that the AP−CaO was more resistant to sintering than the CP−CaO.

These results are very interesting since *particle* size (not necessarily crystallite size) calculated from BET surface areas of CaO are very similar, and yet crystallite sizes by XRD (after 500 °C treatment) are about twice as large for CP−CaO.

2. Gases. Gases evolved during heat treatment were trapped and analyzed by infrared spectroscopy. Figure 6 shows the gaseous products coming off from the autoclave-prepared sample. At 120 °C water (∼1600 cm^{-1}), carbon dioxide (doublet ∼2345 cm^{-1}) and some physisorbed hydrocarbons were evolved. At 300 °C more hydrocarbons (multiple at ∼2900 and ∼1030

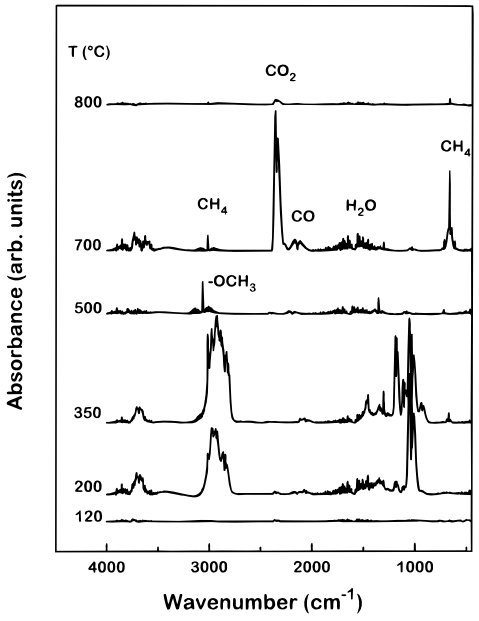

Figure 6. Gaseous products coming off during AP−CaO heat treatment, as detected by IR at room temperature.

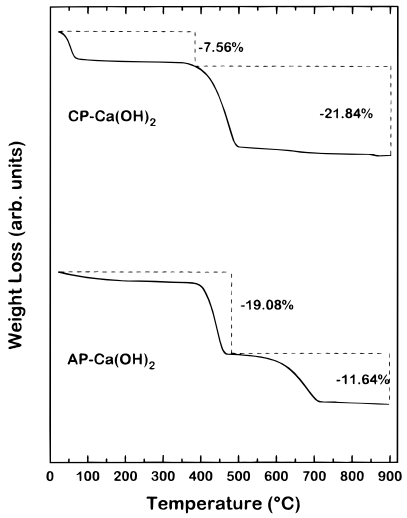

Figure 7. Weight loss for CP− and AP−CaO during heat treatment under helium flow.

cm^{-1}), a small amount of CO_2 and traces of CO (2143 cm^{-1}) were observed. When the temperature was increased to 350 °C, more hydrocarbons as well as methane (3015 and 1034 cm^{-1}) were released. At 500 °C the major products were methane and carbon monoxide (due to residual surface methoxy groups decomposing). At 700 and 800 °C the major peaks were due to carbon dioxide; however, methane and carbon monoxide were still present. These results were corroborated by mass spectrometry. Similar studies of CP−CaO showed water and CO_2 loss. For both samples, carbonate bands in the solid persisted until 800 °C for AP−CaO and above 800 °C for CP−CaO.

3. Weight Loss and Surface Area Changes. Figure 7 shows the weight loss under helium flow, whereas Figure 8 shows the weight loss under air flow. The total weight loss was about the same for both oxides, approximately 30%, and did not differ significantly depending on the environment, helium versus air. In case of CP−CaO there were two major weight losses: from room temperature to 100 °C (lost of physisorbed water)

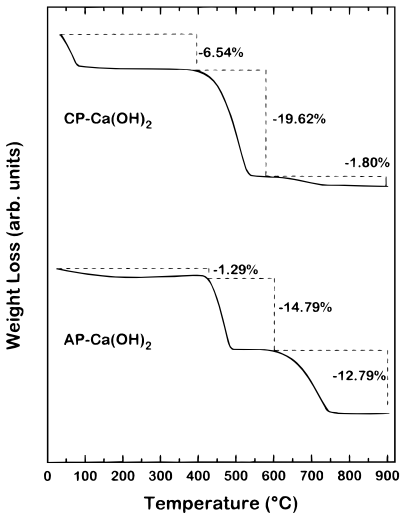

Figure 8. Weight loss for CP− and AP−CaO during heat treatment under air flow.

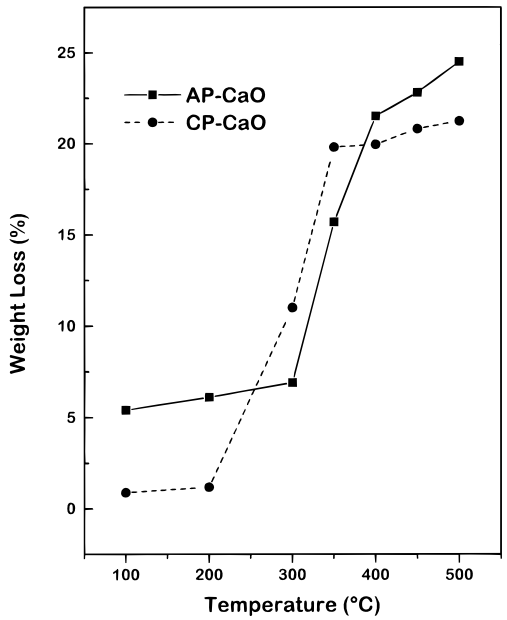

Figure 9. Weight loss for CP− and AP−CaO during heat treatment under vacuum.

and from 380 to 520 °C (lost of chemisorbed water). At higher temperatures 500−900 °C the weight loss was very small, below 2%. The AP−CaO contained much less physisorbed water. Chemisorbed water came off in the 390−450 °C range. The next major weight loss for AP−CaO was at 550−740 °C. On the basis of the IR and MS studies, CO_2, CO, and water were evolved. The high-temperature weight loss was slightly higher for AP−CaO in air than under He flow.

Interestingly, weight loss under dynamic vacuum was considerably different than under normal gas flow TGA conditions (compare Figures 7, 8, and 9). Weight loss under vacuum (Figure 9) showed the same trends as surface area increases (Figure 10).

Indeed as we have reported earlier,[33] under dynamic vacuum a "blossoming" occurs and surface areas of the forming CaO are surprisingly high. The AP−$Ca(OH_2)$ → AP−CaO conversion caused a 2-fold increase in surface area (starting out at a relatively high value), while the CP−CaO system increased 10-fold (Figure 10). By 300 °C the surface areas were comparable, but the

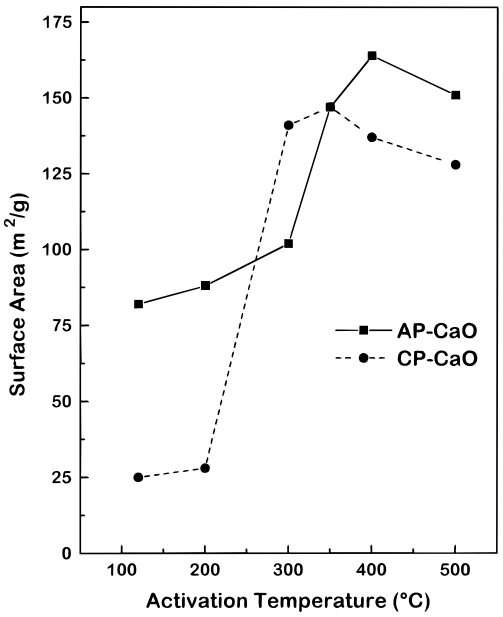

Figure 10. Surface area changes for CP− and AP−CaO during heat treatment under vacuum.

Table 1. Surface −OH Groups on AP− and CP−CaO Determined by $AlEt_3$ Titration

pretreatment temp (°C)	OH/nm²	
	AP−CaO	CP−CaO
300	9.3	8.6
350	6.3	6.9
400	5.6	5.6
500	4.1	3.7

Table 2. Elemental Analysis for AP− and CP−CaO (after 500 °C Heat Treatment under Vacuum)

element	AP−CaO	CP−CaO	calcd
calcium	58.6	65.2	71.43
carbon	0.67	less than 0.5	
hydrogen	1.35	0.75	
oxygen (by difference)	39.4	34	25.57

CP−CaO then began sintering at a lower temperature than AP−CaO.

4. Surface Hydroxyl Groups. Quantitative determination of surface hydroxy groups was possible by titration with $AlEt_3$.[33] Both AP− and CP− samples exhibited similar numbers of surface −OH groups (Table 1).

C. Physical Characterization of CaO Samples.

1. Elemental Analyses. Table 2 shows analyses for AP− and CP− samples after heat treatment at 500 °C under vacuum.

In both cases calcium is low and oxygen is high. For AP−CaO the presence of residual −OH, some $-OCH_3$, and some carbonate may explain these results. For CP−CaO residual −OH and some carbonate were obviously present.

2. Electron Probe Microanalysis (EPMA). Three elements were analyzed. The micrographs indicated a slightly higher surface concentration of Ca ions, and a considerably larger C surface concentration for the AP−CaO vs the CP, essentially in agreement with the bulk elemental analysis results.

3. X-ray Photoelectron Spectroscopy (XPS). Spectra were obtained for the core as well as the valence band region. Comparison spectra for the AP− and CP−CaO samples are shown in Figure 11. Literature values for

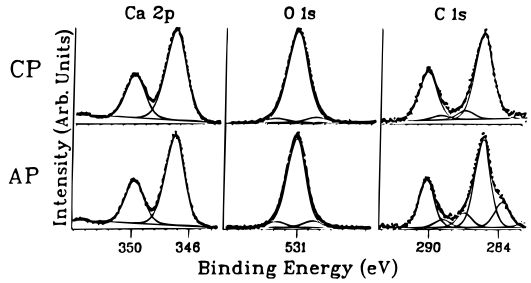

Figure 11. X-ray photoelectron spectra in the core region of CP− and AP−CaO preheat treated at 500 °C.

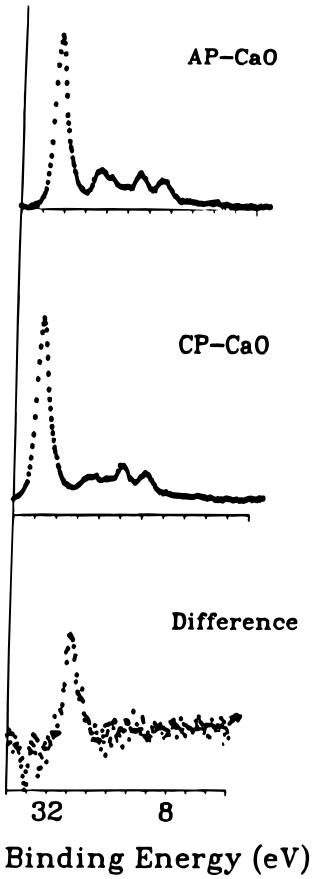

Figure 12. XPS spectra for the valence band region of AP−CAO (top), CP−CaO (middle), and the difference (bottom).

Table 3. Surface Elemental Ratios Calculated from XPS Spectra

	area ratios	
	AP−CaO	CP−CaO
C/Ca	0.397	0.335
O/Ca	0.956	1.03
O/C	2.41	3.09

calcium absorbance are as follows: calcium oxide $2p_{3/2}$ 347.3 eV, in calcium carbonate $2p_{3/2}$ 347.0 eV.[45−47] For oxygen, adsorbed water gives a peak at 534−5 eV, hydroxide at 531 eV, and calcium oxide at 529 eV. In Figure 11 the O 1s peak is at 531 eV; therefore, it can be concluded that the surface is hydroxylated. Oxygen and calcium regions look almost the same, but a difference is apparent in the C 1s region. The peak at 284.6 eV is due to hydrocarbons adsorbed on the surface and is always present in the spectra. The smaller C 1s peak at 290 eV is associated with carbonate species on the surface. In the AP−CaO spectrum an additional feature is seen at 283.5 eV, and it is attributed to

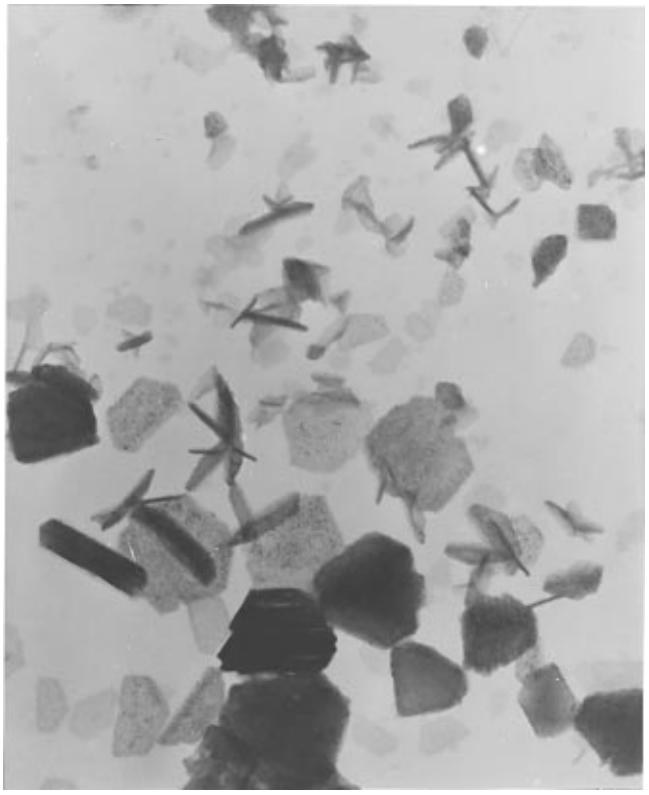

Figure 13. Transmission electron microscope (TEM) picture of CP−CaO. 100 nm = 4.5 mm.

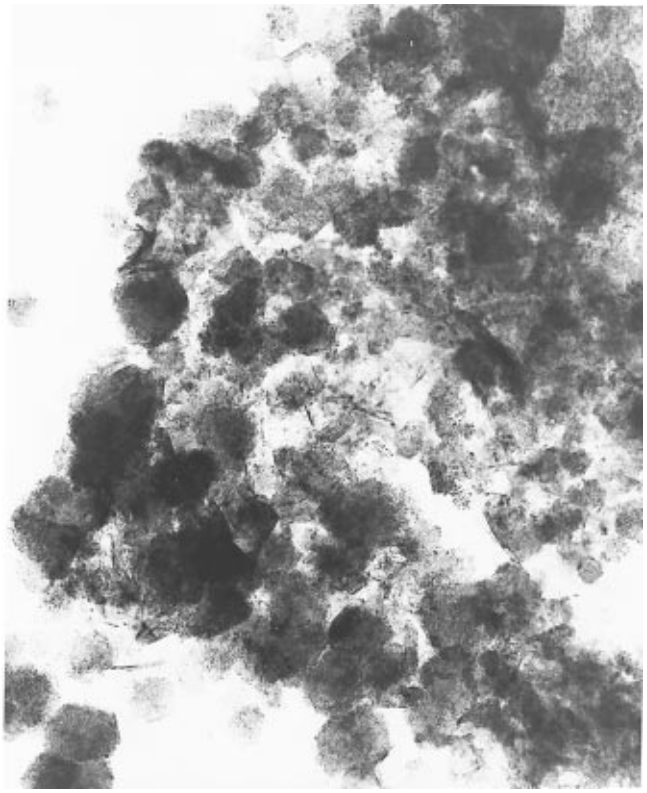

Figure 14. TEM picture of AP−CaO. 100 nm = 4.5 mm.

methoxy groups on the surface.[48] From the areas under the peaks (in the core region) the atomic ratios of elements were calculated and are shown in Table 3. Comparing AP− and CP−CaO, it can be concluded that

(48) Wyckoff, R. W. G. *Crystal Structures*, 2nd ed.; Interscience Publishers: New York, 1963; Vol. 5, pp 64−5.

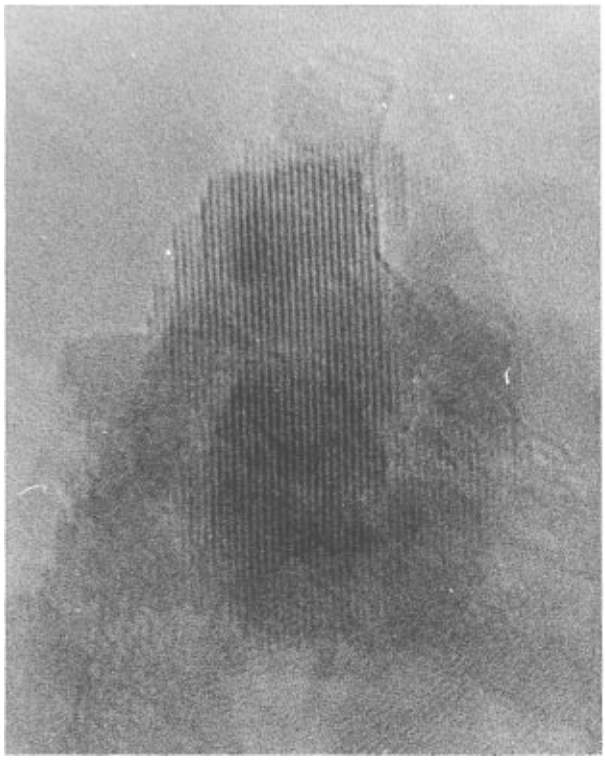

Figure 15. High-resolution TEM of AP−MgO. 1 nm = 5 mm.

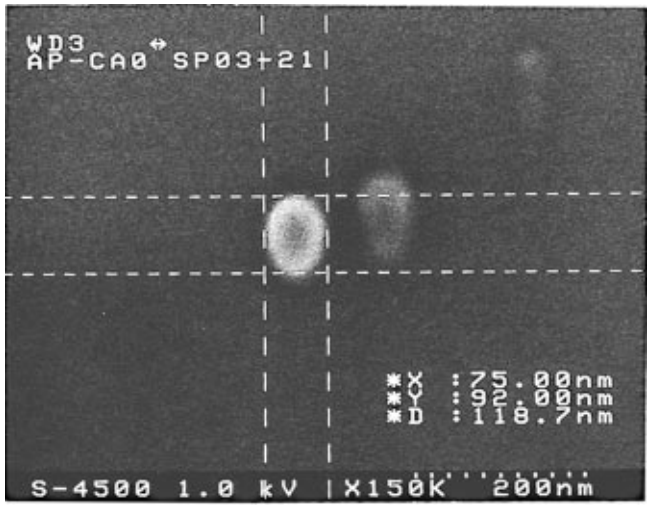

Figure 16. SEM micrograph of AP−CaO.

Table 4. Pore Area, Volume, and Size for CP− and AP−CaO

property	CP−CaO	AP−CaO
single-point surface area at P/P_0 0.2099	87.7 m^2/g	73.3 m^2/g
BET surface area	89.7 m^2/g	75.2 m^2/g
BJH cumulative adsorption surface area of pores between 17 and 3000 Å diam	119.6 m^2/g	92.6 m^2/g
BJH cumulative desorption surface area of pores between 17 and 3000 Å diam	135.5 m^2/g	103.2 m^2/g
single-point total pore vol	0.474 cm^3/g	0.603 cm^3/g
BJH cumulative adsorption pore vol of pores between 17 and 3000 Å diam	0.418 cm^3/g	0.524 cm^3/g
BJH cumulative desorption pore vol of pores between 17 and 3000 Å diam	0.476 cm^3/g	0.604 cm^3/g
av pore diam (4V/A by BET adsorption)	211.4 Å	320.5 Å
av pore diam (4V/A by BJH adsorption)	139.8	226.3
av pore diam (4V/A by BJH desorption)	140.6	234.1

the ratio of C/Ca is greater in the case of aerogel-prepared oxide (as was seen from microprobe experiments); the O/Ca ratios are almost the same for both oxides, being slightly larger for CP−CaO, whereas the

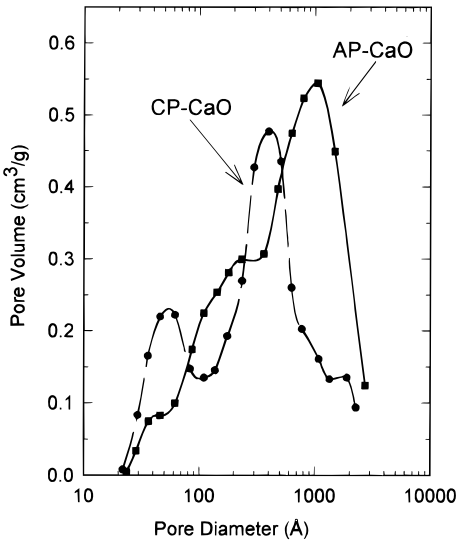

Figure 17. Pore volume distribution for CP− and AP−CaO (after 500 °C preheat treatment).

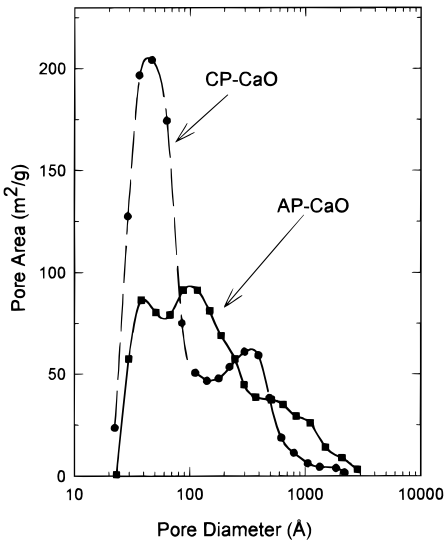

Figure 18. Pore area distribution for CP− and AP−CaO (after 500 °C preheat treatment).

ratio O/C is larger for CP−CaO. This suggests that conventionally prepared oxide has more CO_2 on the surface.

A great deal of qualitative information was obtained from the valence band region. Figure 12 shows three spectra: the top one represents the valence region for AP−CaO, the middle one for CP−CaO, and the bottom one is a difference spectrum between AP− and CP− samples, after subtracting the nonlinear background. The largest peak around 26 eV is due to Ca 3p of Ca^{2+}. This peak overlaps with the O 2s peak, which makes a broad shoulder on the higher energy side. Two broad peaks at 6.4 and 10.6 eV are assigned to CO_3^{2-} species.[47,49] The calcium peak as well as carbonate features are almost the same as for conventionally and aerogel-prepared oxides. However, peaks at the satellite position are much larger for AP−CaO. After subtracting the CP spectrum from the AP spectrum, almost all peaks can be eliminated, except for the large feature around 17 eV with a shoulder at the higher energy side.

(49) Sherwood, P. M. A. *J. Vac. Sci. Technol.*, in press.

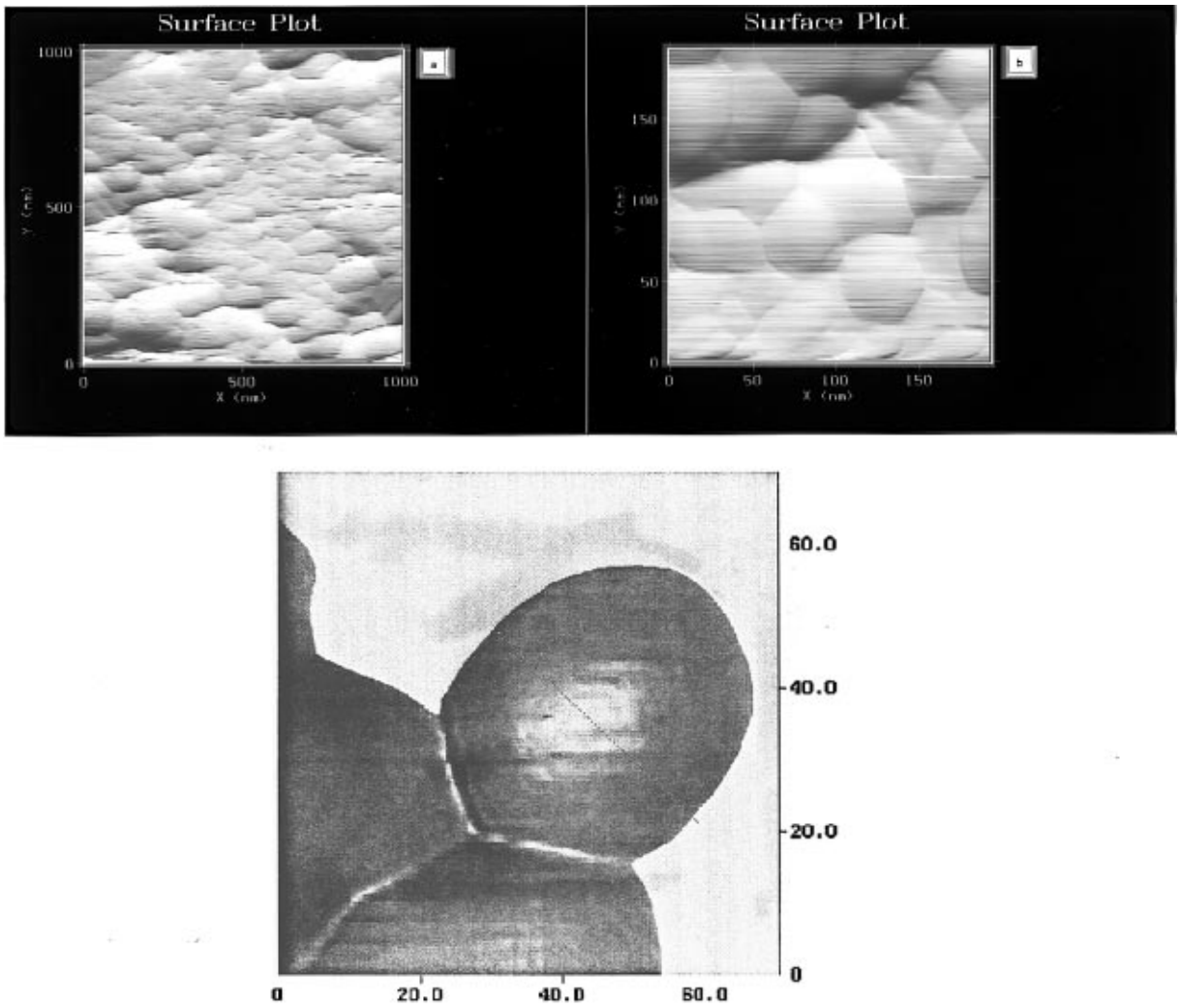

Figure 19. AFM images of (a) CP−CaO powder (1000 × 1000 nm); (b) CP−CaO packed down (200 × 200 nm), and (c) CP−CaO AFM tapping mode (70 × 70 nm).

This peak was assigned to methoxy species on the surface of the AP−oxide.

4. Transmission Electron Microscopy (TEM). It is exceedingly difficult to obtain high-resolution TEM photographs of CaO and MgO fine particles due to the comparatively low electron densities and their insulator properties. For the CaO samples sonication in acetone, ethanol, toluene, or pentane allowed better separation of agglomerated crystallites but also could possibly change their morphologies. After numerous experiments, the best images were obtained using pentane solvent with a sonication time of 60 min.

For the CP−MgO and CP−CaO hexagonal platelets, trigonal pyramids, and cubes were the most common structures (Figure 13), and crystal edges and planes were evident. Particle size ranged from 100 to 300 nm (recall the average crystallite size according to XRD was 14 nm).

In the case of AP−CaO and AP−MgO weakly agglomerated porous particles were observed. Hexagonal ordering was often observed, but crystallite sizes were smaller (7 nm for AP−CaO and 4 nm for AP−MgO). Figure 14 illustrates these porous ordered particles for AP−CaO. Only in the case of AP−MgO was a good-quality high-resolution image obtained (Figure 15), and the lattice planes are clearly evident.

In the case of AP−CaO the better image was obtained by a high-resolution SEM technique FESEM, and a single particle is shown in Figure 16, which is oval in shape, shows no crystal edges, and is about 50 × 90 nm (7 nm internal crystallite size).

5. Pore Size Distribution (BET and BJH Methods). The summary of the results for the pore area, pore volume, and pore size is shown in Table 4. Two methods were used to obtain these data: the Brunauer−Emmet−Teller method (BET) and the Barret−Joyner−Hallenda (BJH) numerical integration method.[50−55] The pore volume and area distribution are shown in Figures 17 and 18, respectively. As can be seen in these two types of calcium oxides, overall surface areas were very similar.[56] (In fact, with these samples, after appropriate heat treatment in order to prepare them for the adsorption studies, the CP−CaO surface area actually was slightly larger than the AP−CaO. Usually AP−samples have slightly higher surface areas, generally AP−CaO 120−160 and CP−CaO 80−100. In the case of AP−

(50) Micromeritics Service Manual for FlowSorb II, 2300.
(51) Lowell, S. *Introduction to Powder Surface Area*; John Wiley & Sons: New York, 1979.
(52) Jura, G.; Harkins, W. D. *J. Chem. Phys.* **1943**, *11*, 430.
(53) Anderson, R. B. *J. Catal.* **1964**, *3*, 50.
(54) Lippens, B. C.; Boer, J. H. *J. Catal.* **1965**, *4*, 319.
(55) Barret, E. P.; Joyner, L. G.; Halenda, P. P. *J. Am. Chem. Soc.* **1951**, *73*, 373.
(56) Decker, S.; Klabunde, K. J. *J. Am. Chem. Soc.* **1996**, *118*, 12465−12466.

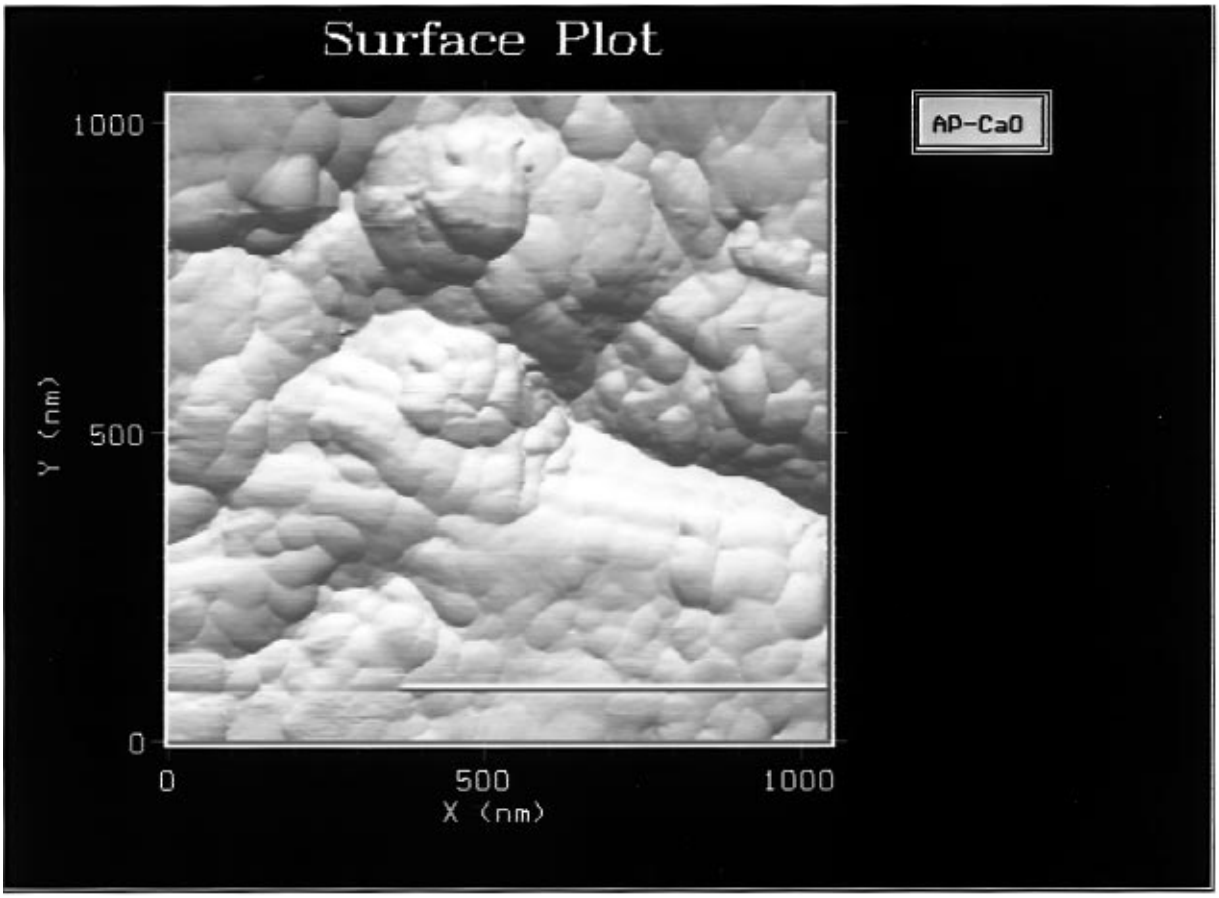

Figure 20. AFM image of AP−CaO packed down (1000 × 1000 nm).

MgO vs CP−MgO, the AP− samples are usually much higher in surface area, e.g., 400 m^2/g for AP with 150 m^2/g for CP.[9])

Despite the similarities in surface areas, the AP−CaO exhibited much larger pore volume and pore size. Three pore size ranges could be distinguished: 35, 115, and 1000 Å for AP−CaO, whereas for CP−CaO two sharp maxima were observed at 55 and 400 Å. It is very interesting to note that the pore *area* for CP−CaO is larger than for AP−CaO for the smaller pores.

6. Atomic Force Microscopy (AFM). **CM−CaO:** The surface of commercial CaO was first studied as a pellet, and the surface displayed many flat areas. The particles were elongated in shape, and their size was around 90 nm. The same sample was then observed as a powder slightly packed down and exhibited a size distribution ranging from 30 to 80 nm. **CP−CaO:** A difference in the particle size was observed for loose powder (31−33 nm) or as a pressed pellet (41−43 nm, Figure 19a,b). In both cases, the particles were slightly elongated in shape. The CP−CaO sample surface was also observed by AFM using the tapping mode (Nanoscope III from Digital Instruments Inc.). The experiment was carried out on pressed CP−CaO. Figure 19c shows the detail of a CP−CaO particle. In this figure, the elongated shape of the particle can be clearly seen, and the particle size was 40 nm. **AP−CaO:** The aerogel-prepared sample surface exhibited aggregates varying in size from 60 to 100 nm (Figure 20). These aggregates were made up of small spherical particles with a size distribution ranging from 20 to 40 nm, most being near 25 nm. These data were recorded on a powdered sample slightly packed down. An AP−CaO sample surface observed after being pressed into a pellet showed larger aggregates with poorer resolution.

Table 5. Amounts of Pyridine and Carbon Dioxide Adsorbed by CaO Samples at Room Temperature

sample	surface area (m^2/g)	molecules adsorbed/nm^2	
		Py[a] (4 Torr)	CO_2[b] (10 Torr)
AP−CaO	120	1.0	5.2
CP−CaO	98	1.7	5.8

[a] Monolayer coverage is calculated to be 13.2/nm^2 for N bound upright and 3.3/nm^2 for lying flat. [b] Monolayer coverage is calculated to be 5.1 (19.5 $Å^2$ for each CO_2 molecule).

7. Acidity and Basicity. Upon adsorption of pyridine, white calcium oxide turned purple, and upon evacuation, the color faded but did not disappear completely. In the carbon dioxide adsorption experiment, the color of the sample did not change upon adsorption. Quantitative determination of the amounts of CO_2 and pyridine adsorbed was carried out on a quartz spring balance at room temperature (following 500 °C preheat treatment under vacuum). Table 5 summarizes the data.

These data indicate that the CO_2 is bound as a monolayer on both AP− and CP−CaO. Compared with analogous MgO samples, these CaO samples are considerably more basic.[13]

For pyridine, adsorption is less than a monolayer, and may involve adsorption only to Bronsted acid sites (surface −OH groups). Indeed, infrared spectroscopy supported this idea. After adsorption of pyridine at 4 Torr for 15 min followed by evacuation, two absorptions were observed: 1596.7 (s) and 1444 (vs) cm^{-1}. From the literature hydrogen-bonded pyridine shows bands

Table 6. Summary of General Features of AP− vs CP−CaO Particles

	AP−CaO (aerogel prepared)	CP−CaO (conventionally prepared from $Ca(OH)_2$)	CM−CaO (commercially) available, from $CaCO_3$ thermal decomposition
surface areas	80−160	60−100	10
pore vol	0.60 cm^3/g	0.48 cm^3/g	
pore area		larger for small pores	
pore diam	larger		
AFM	spherical aggregates 25 nm	elongated aggregates 33 nm	
thermal stability toward sintering	higher		
residual surface −OH	isolated −OH at 500 °C, 4.1/nm^2	isolated −OH at 500 °C, 3.7/nm^2	
residual $-OCH_3$	stable up to 700 °C		
carbon content	higher		
CO_2 adsorption	more unidentate	more bidentate	
pyridine adsorption	on Bronsted sites	on Bronsted sites, slightly more adsorbed	

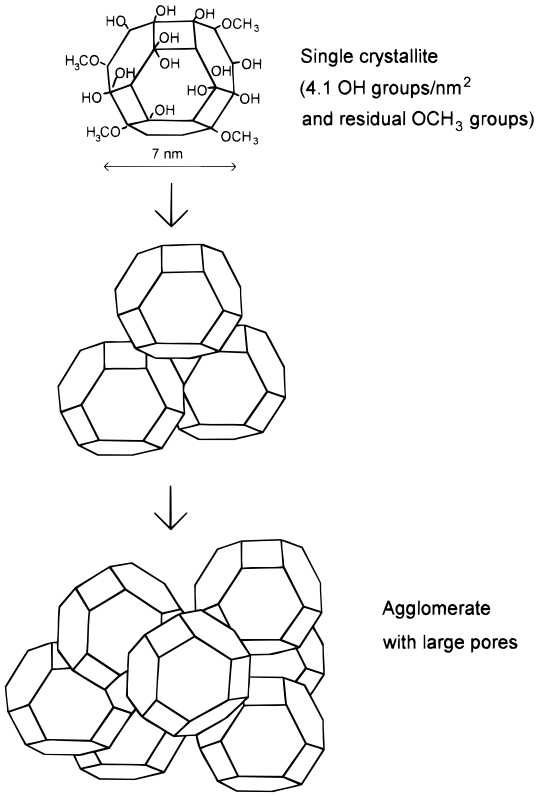

Figure 21. Model of AP−CaO particle.

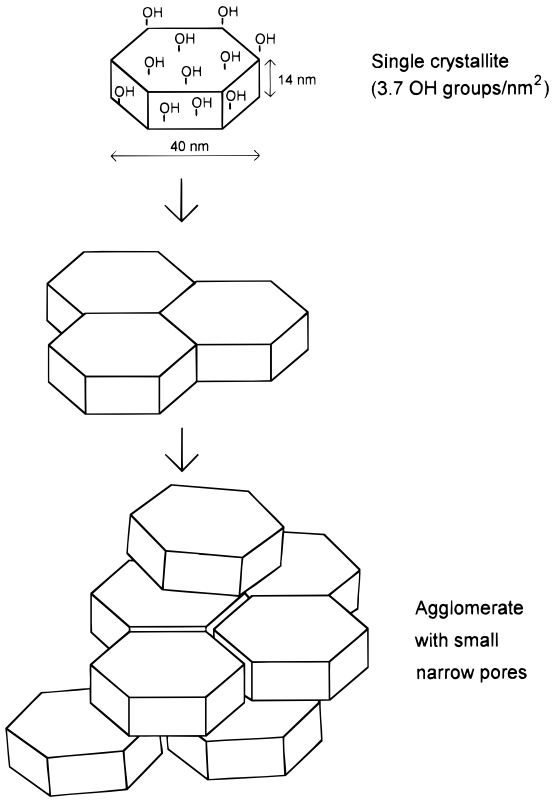

Figure 22. Model of CP−CaO particle.

at 1440−1447 (vs), 1450−1490 (w), and 1580−1600 (s) cm^{-1}.[21] Similar studies for CO_2 adsorption after evacuation gave samples exhibiting one new band at 2367 cm^{-1}.

Discussion

A modified aerogel−hypercritical drying method has resulted, after vacuum dehydration, in CaO in an ultrafine particulate form of high surface area and unexpectedly high surface reactivity with chlorocarbons, acid gases, and organophosphorus compounds.[9−14] An important feature of this modified aerogel procedure is the addition of toluene solvent to the $Ca(OCH_3)_2$−methanol solution, which lowers the overall polarity and surface tension of the solvent mix and results in the formation of considerably higher surface areas.

The vacuum dehydration step is also an important feature, and both aerogel $Ca(OH)_2$ and the more conventionally prepared $Ca(OH)_2$ dehydrated to form higher surface area CaO. This "blossoming" behavior has been observed before for $MgCO_3$[47], and $Mg(OH)_2$,[7,12,31,33] and is particularly striking in the case of $Ca(OH)_2$. During $Ca(OH)_2$ dehydration under vacuum, where the hot steam is removed quickly, the forming CaO particles break off and "ball-up" to very small sizes without being given a chance for sintering. This unique behavior is dependent on the heat-treatment conditions (rate of heating, pumping speed). Crystallite sizes also decrease during the $Ca(OH)_2 \rightarrow$ CaO conversion, yielding 7 nm AP−CaO and 14 nm CP−CaO. Interestingly, upon heat treatment at 350 °C crystallite sizes are nearly the same (8 nm), but further dehydration at higher temperatures caused crystallite growth in the CP− system, but the AP− system crystallite size decreased even more and was stable at 7 nm at fairly high temperatures (500 °C).

Both samples adsorb CO_2 in unidentate and bidentate carbonate modes. The partial charge of the surface O^{2-} can be compared by measuring the wavenumber difference $\Delta\nu = \nu_{as} - \nu_{sy}$ (asymmetric and symmetric stretching of unidentate carbonate); $\Delta\nu$ decreases with increasing negative charge to which CO_2 is bonded.[39] For CP−CaO, $\Delta\nu$ is approximately 69 cm^{-1} and for AP−CaO 85 cm^{-1}, indicating slightly more negative charge on CP−

CaO (more basic). This result is consistent with the slightly higher amount of CO_2 adsorbed at room temperature (5.8 CO_2/nm^2 for CP−CaO and 5.2 CO_2/nm^2 for AP−CaO). However, we also note that bidentate coordination is more preferred for CP−CaO, while unidentate is for AP−CaO, as was found for analogous MgO samples.[13] Thus, it appears that unidentate adsorption is more prevalent on AP−CaO as well as AP−MgO. In an earlier report we attributed this to morphological differences, where AP− samples possess smaller crystallites with a high ratio of edge/surface ions, while CP− samples have more flat planes more capable of bidentate type bonding.

Another interesting feature is the persistent presence of isolated surface −OH groups on these materials (4.1/nm^2 and 3.7/nm^2 for AP− and CP−CaO at 500 °C under vacuum with a few still remaining even up to 800 °C). These isolated −OH structures are very stable especially on the AP− system. Perhaps ever more remarkable is the persistent presence of surface $-OCH_3$ groups as detected by IR, XPS, and elemental analyses. These groups are present as a residue of the preparation from $Ca(OCH_3)_2$, and they are surprisingly chemically and thermally stable, having survived 265 °C in an autoclave with a slight molar excess of H_2O present, and stable upon heating AP−CaO samples under vacuum up to 700 °C.

Additional physical characterizations of the samples by TEM, SEM, and gas adsorption experiments illustrated that the AP− samples were less crystalline with particle sizes of 25 nm for AP and 33 nm for CP. The pore volume and pore diameters of the AP− samples were much larger compared with CP− and commercial samples, but pore area was larger for smaller pores in CP−CaO.

A table summarizing these findings is helpful in attempting to develop models for aerogel prepared nanoparticles vs conventionally prepared and commercial samples (Table 6).

In earlier reports describing aerogel prepared MgO vs more conventional samples, it was possible to propose contrasting morphological models since surface areas, crystallite sizes, porosity, and adsorption and chemical reactivity behaviors were vastly different.[9,13,33] However, in the case of CaO it has not been possible to isolate materials with such huge surface areas, and AP− and CP− samples are actually similar in surface areas (although CM−CaO is a factor of 10 lower than both). Nonetheless, the AP− and CP− samples do behave differently in surface chemical reactivity and porosity, and so these materials must have different surface morphologies. Illustrated in Figures 21 and 22 are models that perhaps can help explain these differences.

We propose that the residual surface −OH and $-OCH_3$ groups help stabilize the AP−CaO crystallites toward crystal coalescence. However, three or four crystallites aggregate into ∼25 nm particles, and these particles weakly agglomerate into a mass with large pores, where the pores are actually the space between the particles (as opposed to holes and channels in the particles themselves). The existence of these large pores, the small crystallite size, and the presence of the residual −OH and $-OCH_3$ groups allow more effective penetration of reagents into the inner reaches of the particles during destructive adsorption processes described earlier.[10,12]

In the case of the CP−CaO flatter, more elongated particles of larger crystallite size must tightly aggregate together to give a mass of material with smaller, narrower pores. The tighter pores and larger crystallite sizes allow for a little less penetration of incoming reagents, such as chlorocarbons or other relatively large molecules.

It should be noted, however, that small molecules such as CO_2 can easily gain access to the pores of both AP− and CP−CaO and, as shown herein, similar adsorption capacities were observed at room temperature. On the other hand, at higher temperatures, for example SO_2 chemisorption $CaO + SO_2 \rightarrow CaSO_3$, AP−CaO once again exhibits superior properties.[56]

Acknowledgment. The support of the Army Research Office and the Hazardous Substance Research Center is acknowledged with gratitude.

CM970357A